Role of Conserved Aspartates in the ArsA ATPase[†]

Hiranmoy Bhattacharjee,* Ranginee Choudhury,[‡] and Barry P. Rosen

Department of Biochemistry and Molecular Biology, Wayne State University School of Medicine, Detroit, Michigan 48201

Received April 22, 2008; Revised Manuscript Received May 23, 2008

ABSTRACT: The ArsA ATPase is the catalytic subunit of the arsenite-translocating ArsAB pump that is responsible for resistance to arsenicals and antimonials in *Escherichia coli*. ATPase activity is activated by either arsenite or antimonite. ArsA is composed of two homologous halves A1 and A2, each containing a nucleotide binding domain, and a single metalloid binding or activation domain is located at the interface of the two halves of the protein. The metalloid binding domain is connected to the two nucleotide binding domains through two DTAPTGH sequences, one in A1 and the other in A2. The DTAPTGH sequences are proposed to be involved in information communication between the metal and catalytic sites. The roles of Asp142 in A1 D_{142}TAPTGH sequence, and Asp447 in A2 D_{447}TAPTGH sequence was investigated after altering the aspartates individually to alanine, asparagine, and glutamate by site-directed mutagenesis. Asp142 mutants were sensitive to As(III) to varying degrees, whereas the Asp447 mutants showed the same resistance phenotype as the wild type. Each altered protein exhibited varying levels of both basal and metalloid-stimulated activity, indicating that neither Asp142 nor Asp447 is essential for catalysis. Biochemical characterization of the altered proteins imply that Asp142 is involved in Mg^{2+} binding and also plays a role in signal transduction between the catalytic and activation domains. In contrast, Asp447 is not nearly as critical for Mg^{2+} binding as Asp142 but appears to be in communication between the metal and catalytic sites. Taken together, the results indicate that Asp142 and Asp447, located on the A1 and A2 halves of the protein, have different roles in ArsA catalysis, consistent with our proposal that these two halves are functionally nonequivalent.

Arsenic is widely distributed throughout the earth's crust and is found in water that flowed through arsenic-rich rocks. Severe health effects have been observed in populations exposed to arsenic, which include cancer, cardiovascular disease, peripheral neuropathies and diabetes mellitus (*1*). Because of the prevalence of arsenic in the environment, nearly every organism, from *Escherichia coli* to humans, has genes for arsenic detoxification (*2*). The ArsAB pump in *E. coli*, encoded by the *ars* operon of plasmid R773, confers resistance to arsenicals and antimonials. ArsA[1] is the catalytic subunit of the pump that hydrolyzes ATP in the presence of arsenite [As(III)] or antimonite [Sb(III)]. ATP hydrolysis is coupled to extrusion of As(III) or Sb(III) through ArsB, which serves both as a membrane anchor for ArsA and as the substrate-conducting pathway (*3*). Upon overexpression, ArsA exists primarily as a soluble protein in the cytosol. Purified ArsA is an As(III)/Sb(III)-stimulated ATPase (*4*).

ArsA is composed of homologous N-terminal (A1) and C-terminal (A2) halves that are connected by a short linker (*5*). Each half contains a consensus sequence for a nucleotide-binding domain (NBD), and both NBDs are required for ATPase activity and metalloid transport (*6, 7*). The NBDs are formed by residues from both the A1 and A2 halves of the protein (*8*). A novel metalloid-binding domain (MBD), located at the A1−A2 interface diametrically opposite to the NBDs, allosterically modulates ATPase activity (*9*). The MBD contains one or more metalloid atoms that are coordinated to one residue from the A1 half and another from the A2 half of the protein (*8*). Thus metalloid serves as the "molecular glue" that holds the two halves of the protein together, forming the interface at the NBDs, activating catalysis. It has been proposed that conformational changes associated with nucleotide hydrolysis alter the affinities of the metalloid atoms bound at MBD, which are then injected into ArsB and extruded from the cell (*8, 10*).

In the absence of metalloid, a condition that promotes basal hydrolysis, both NBD1 and NBD2 bind and hydrolyze ATP, albeit at a slow rate (*11*). In the presence of metalloid, ATP hydrolysis is stimulated in both NBD1 and NBD2, with hydrolysis at NBD1 stimulated to a greater degree than at NBD2 (*11*). These properties suggest that the two NBDs have different properties, and may therefore have different functions. The crystal structure of ArsA shows that Asp142 at NBD1 and Asp447 at NBD2 are in close proximity to the magnesium ions of the MgADP substrates (Figure 1). Asp142 is indirectly coordinated to the Mg^{2+} at NBD1 by its

[†] This work was supported by National Institutes of Health Grant GM55425.

* Author to whom correspondence should be addressed. E-mail: hbhattac@med.wayne.edu. Tel: (313) 577-4182. Fax: (313) 577-2765.

[‡] Present address: The Department of Animal and Poultry Sciences, College of Agriculture and Life Sciences, Virginia Tech, Blacksburg, VA 24061.

[1] Abbreviations: ArsA, catalytic subunit of the arsenite transporter; ArsB, membrane channel of the arsenite transporter; A1, N-terminal half of ArsA; A2, C-terminal half of ArsA; AMP-PNP, adenosine 5′-(β,γ-imido)triphosphate; Bis-tris propane, 1,3-Bis[tris(hydroxymethyl)-methylamino]propane; IPTG, isopropyl β-D-thiogalactoside; MOPS, 4-morpholinepropanesulfonic acid; MBD, metalloid binding domain; NBD, nucleotide binding domain; STD, signal transduction domain; SDS−PAGE, sodium dodecyl sulfate−polyacrylamide gel electrophoresis.

10.1021/bi800715h CCC: $40.75
Published on Web 06/14/2008

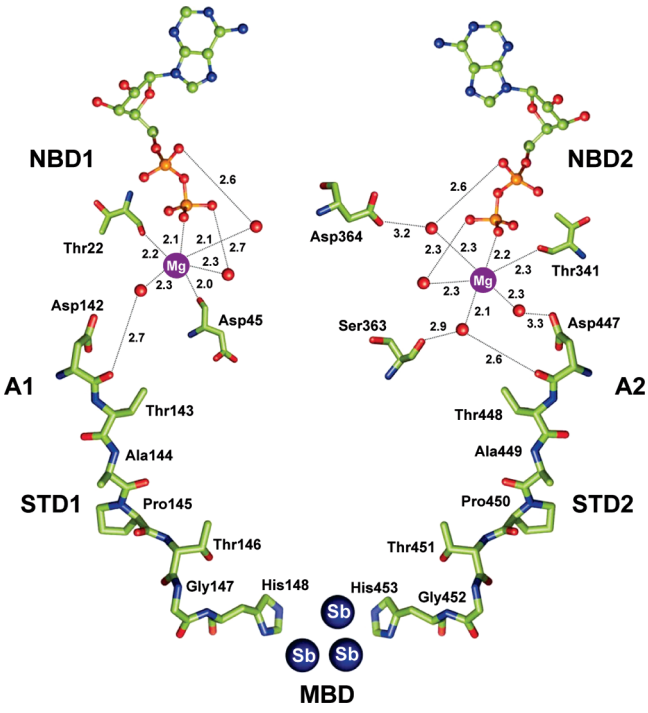

FIGURE 1: Domains of the ArsA ATPase. The A1 and A2 STDs, two stretches of seven residues with the identical sequence $D_{142/447}TAPTGH_{148/453}$, connect the single MBD to the A1 and A2 MgADP-filled NBDs (*8*). The nucleotides bound in the two NBDs are shown as ball-and-stick models colored according to atom type (phosphorus, orange; oxygen, red; nitrogen, blue). The DTAPTGH sequences are shown as stick models with green bonds. Sb(III) (blue), Mg^{2+} (magenta), and water (red) are shown as space-filling models. Asp142 and Asp447, representing the N-terminal ends of the STDs, coordinate indirectly to the Mg^{2+} ions in NBD1 and NBD2, respectively, through water molecules. The octahedral Mg^{2+} coordination is indicated, and the distances are expressed in angstroms. Two of the three metalloids in the MBD are liganded to the imidazole nitrogen in His148 and His453.

backbone carbonyl through a hydrogen bonded water molecule. Similarly, the Mg^{2+} at NBD2 is indirectly coordinated by water molecules that form hydrogen bonds with both the backbone and the carboxylate of Asp447 (*8*). In addition, each Mg^{2+} has a number of additional coordinations. The Mg^{2+} at NBD1 is coordinated to Thr22, Asp45, the β-phosphate of ADP, and indirectly to the α-phosphate of ADP through a water molecule. Asp45 has been previously identified as a Mg^{2+} ligand (*12*). The Mg^{2+} at NBD2 is coordinated to Thr341 and indirectly through water molecules to Ser363, Asp364, and the α- and β-phosphates of ADP. Structures of ArsA with ATP, the nonhydrolyzable ATP analogue, AMP-PNP, or the transition state analogue of ATP hydrolysis, ADP·AlF_3, bound at NBD2 have also been determined. These structures indicate that binding of different nucleotides produces subtle distortions in the coordination geometry of Mg^{2+} at NBD2, which may be essential for ATP hydrolysis (*10*). Additionally, movement of amino acid side chains at NBD2 during ATP binding and hydrolysis produces large positional shifts at NBD1, indicating extensive cross-talk between NBD1 and NBD2 (*10*).

Asp142 and Asp447 are located at the N-terminal end of an elongated stretch of residues, $D_{142}TAPTGH_{148}$ in A1 and $D_{447}TAPTGH_{453}$ in A2 forming the signal transduction domains (STDs) that physically connects the two NBDs to the single MBD and may be the primary effector of signal transduction between these centers (*8*). His148 and His453, located at the C-terminal end of the STDs, have been shown to be involved in transmission of information of metalloid occupancy in the single MBD to the two NBDs during catalysis (*13*), and in the crystal structure these two histidines can be seen to be ligands to two of the metalloids in the MBD (*8*), although the biochemical function of these two metalloids is not clear (*9*). The objective of this study was to determine what role the two aspartates (Asp142 and Asp447) play in Mg^{2+} binding, signal transduction, and catalysis. The results presented here suggest that the two aspartates have different functions.

EXPERIMENTAL PROCEDURES

Growth of Cells. *E. coli* strains and plasmids used in this study are described in Table 1. Cells were grown in Luria−Bertani medium (*14*) at 37 °C. Ampicillin (125 μg/mL), tetracycline (12.5 μg/mL), and IPTG (0.1 mM) were added as required.

Site-Directed Mutagenesis. Mutations in the *arsA* gene were introduced by site-directed mutagenesis using the Altered Sites II *in vitro* Mutagenesis Systems (Promega) with plasmid pTZ3H6 containing the *arsA* and *arsB* genes (*15*). In this plasmid the *arsA* gene was previously mutated to contain only a single tryptophan codon (Trp159), and the sequence for six histidine codons was added at the 3′ end. This plasmid was used as the template to produce *arsA* mutants with D142A, D142E, D142N, D447A, D447E, and D447N substitutions. The mutagenic oligonucleotides containing the respective changes (underlined) are as follows: D142A, 5′-CGT CGG CGC GGT AGC AAA AAT GAT AT-3′; D142E, 5′-CGT CGG CGC GGT CTC AAA AAT GAT AT-3′; D142N, 5′-CGT CGG CGC GGT ATT AAA AAT GAT AT-3′; D447A, CGG AGC CGT AGC CAT CAC CAC; D447E, CGG AGC CGT TTC CAT CAC CAC; D447N, CGG AGC CGT ATT CAT CAC CAC.

DNA Manipulation and Sequence Analysis. Plasmid DNA was purified using QIAprep Spin Miniprep Kit (Qiagen). DNA ligation and transformation were performed as described (*14, 16*). All mutations were confirmed by sequencing the entire gene using a CEQ2000 DNA sequencer (Beckman Coulter).

Cellular Localization of Altered ArsAs. Cultures of cells containing the appropriate plasmids were grown in LB medium at 37 °C to an OD600 of 0.6, followed by induction with 0.1 mM IPTG for 3 h. Five hundred microliters of the cell suspension was pelleted and suspended in 100 μL of SDS sample buffer. After boiling for 5 min, the proteins from 2 μL samples were separated by 10% sodium dodecyl sulfate (SDS)−polyacrylamide gel electrophoresis (PAGE) (*17*). Immunoblotting was performed with 6 × His Monoclonal Antibody (Clontech) utilizing the Western Lightning Western Blot Chemiluminescence Reagent (PerkinElmer) and exposed to X-ray film at room temperature.

To determine the cellular location of the expressed proteins, 100 mL of induced cells were pelleted by centrifugation and washed with 10 mM Tris-HCl, pH 7.5, containing 0.1 M KCl. The cells were suspended in 5 mL of a buffer consisting of 25 mM Bis-tris propane, pH 7.5, containing 250 mM NaCl, 1 mM disodium EDTA, 1 mM dithiothreitol, and 20% (v/v) glycerol, and lysed by a single passage

Table 1: Strains and Plasmids

strain/plasmid	genotype/description	ref
E. coli strains		
ES1301 *mutS*	*lac*Z53, *mut*S201::Tn5, *thy*A36, *rha*-5, *met*B1, *deo*C, IN(*rrn*D-*rrn*E)	Promega
JM109	*end*A1, *rec*A1, *gyr*A96, *thi, hsd*R17 (rk−, mk+), *rel*A1, *sup*E44, λ−, Δ(*lac-pro*AB), [F′, *tra*D36, *pro*AB, *lac*I^{q}ZΔM15]	*14*
plasmids		
pALTER-1	cloning and mutagenesis vector, Tc^r, Ap^s	Promega
pALTER-B	1.3 kb *Hin*dIII−*Kpn*I fragment containing the *arsB* gene cloned into the multiple cloning sites of pALTER-1 (*arsB*), Tc^r, Ap^s	(*30*)
pTZ3H6	*arsA* gene with only Trp^{159} codon remaining and with six histidine codons added to 3′-end (*arsA*$_{H6}$*B*), Tc^s, Ap^r	(*15*)
pD142A	site-directed mutagenesis of Asp^{142} codon to alanine codon in *arsA* gene of pTZ3H6 (*arsA*$_{D142A}$*B*), Tc^r, Ap^r	this study
pD142E	site-directed mutagenesis of Asp^{142} codon to glutamate codon in *arsA* gene of pTZ3H6 (*arsA*$_{D142E}$*B*), Tc^r, Ap^r	this study
pD142N	site-directed mutagenesis of Asp^{142} codon to asparagine codon in *arsA* gene of pTZ3H6 (*arsA*$_{D142N}$*B*), Tc^r, Ap^r	this study
pD447A	site-directed mutagenesis of Asp^{447} codon to alanine codon in *arsA* gene of pTZ3H6 (*arsA*$_{D447A}$*B*), Tc^r, Ap^r	this study
pD447E	site-directed mutagenesis of Asp^{447} codon to glutamate codon in *arsA* gene of pTZ3H6 (*arsA*$_{D447E}$*B*), Tc^r, Ap^r	this study
pD447N	site-directed mutagenesis of Asp^{447} codon to asparagine codon in *arsA* gene of pTZ3H6 (*arsA*$_{D447N}$*B*), Tc^r, Ap^r	this study

through a French Press at 20,000 psi, followed by immediate addition of 2.5 μL of the serine protease inhibitor diisopropylfluorophosphate per g wet weight of cells. Insoluble protein bodies were pelleted at 10000*g* for 10 min and suspended in the original volume of the same buffer. Cytosol was produced by removing membranes at 150000*g* for 1 h. Samples (30 μL) were mixed with 10 μL of 4 × concentrated SDS sample buffer and boiled for 5 min. Two microliters of each sample was analyzed by Western blotting.

Purification of [His]$_6$-Tagged ArsA ATPases. Altered ArsAs were purified from cultures of *E. coli* strain JM109 harboring the indicated plasmids (Table 1). Cells were grown at 37 °C in Luria−Bertani medium to an OD600 of 0.6, at which point 0.1 mM IPTG was added to induce ArsA expression. The cells were grown for another 3 h before being harvested by centrifugation. The soluble ArsA proteins were purified as described (*18*). The concentration of altered ArsA proteins in purified preparations was determined from the absorption at 280 nm using an extinction coefficient of 20,250 M^{-1} cm^{-1} for W159H6 ArsA (*15*). ATPase activity was assayed using an NADH-coupled assay method (*19*).

Fluorescence Measurements. Fluorescence measurements were performed using a PTI spectrofluorometer with a built-in magnetic stirrer. The bandwidths for emission and excitation monochromators were 4 nm. Tryptophan fluorescence was monitored with an excitation wavelength of 295 nm and an emission wavelength of 337 nm. The fluorescence of the buffer (50 mM MOPS−KOH, pH 7.5) alone was subtracted from protein spectra. ArsA (1.3 μM), ATP (5 mM), Mg^{2+} (5 mM), and Sb(III) (1 mM) were added as indicated.

Limited Trypsin Digestion of ArsA. Limited trypsin digestion was performed at room temperature in 50 mM MOPS−KOH buffer, pH 7.5 containing 0.25 mM EDTA and 1 mg/mL ArsA. The ArsA: trypsin ratio was 500:1 (w/w). ArsA proteins were incubated with 5 mM ATP, 5 mM Mg^{2+}, and 0.5 mM Sb(III) either alone or in different combinations. Digestion was initiated by the addition of *N-p*-tosyl-L-phenylalanine chloromethyl ketone treated trypsin (Sigma). Proteolysis was terminated at the indicated times by addition of a 10-fold excess of soybean trypsin inhibitor to the reaction mixture (*20*). Samples were analyzed by 12% SDS−PAGE and Coomassie Blue staining.

RESULTS

Effect of Alteration of Asp142 and Asp447 on Metalloid Resistance. Plasmid pTZ3H6 was used as the parental plasmid to create mutation in the *arsA* gene. The *arsA* gene in plasmid pTZ3H6 has a single tryptophan residue at position 159 and a six-histidine tag at its C-terminus but is otherwise wild type (*15*). Resistance conferred by this plasmid was the same as a plasmid bearing the wild type *arsA* gene (*15*), so this modified *arsA* gene was used as the parent strain for all mutations, and will henceforth be referred to as wild type ArsA. Both Asp142 and Asp447 were individually changed to alanine, asparagine, and glutamic acid by site-directed mutagenesis, producing ArsA derivatives D142A, D142N, D142E and D447A, D447N, D447E, respectively (Table 1).

Cells bearing the mutated *arsA* and wild type *arsB* genes were characterized phenotypically for arsenite resistance. Cells expressing wild type *arsA* and *arsB* genes could grow in medium containing 4 mM sodium arsenite; cells without an *ars* operon were sensitive to 0.2 mM sodium arsenite; while cells expressing *arsB* alone were resistant to 0.2 mM but not 1 mM sodium arsenite (Figure 2). Mutational replacement of Asp142 with glutamic acid resulted in a marginal reduction in arsenite resistance compared with the wild type (Figure 2A). Substitution of Asp142 with either alanine or asparagine exhibited a further decrease in resistance (Figure 2A) and exhibited a phenotype intermediate between sensitive and fully resistant cells. In contrast, cells bearing *arsA*$_{D447A}$, *arsA*$_{D447E}$, or *arsA*$_{D447N}$ genes were each as resistant to sodium arsenite as the wild type (Figure 2B).

Expression and Cellular Location of Altered ArsAs. The steady-state level of wild type and altered ArsAs in cells was estimated by Western blot analysis using antiserum to wild type ArsA. Each altered protein was produced in approximately the same amount and migrated with the same mobility as wild type ArsA (data not shown). The cellular location of the altered proteins was determined. Although ArsA is functionally a component of the membrane-bound pump, it is found in the cytosol when highly expressed (*4*). D142A, D142E, and D142N ArsAs were found predominantly in the cytosol at similar levels as the wild type (data not shown). In contrast, a major portion of D447A and D447E proteins were found as insoluble aggregates, while only trace amounts of D447N could be observed in the soluble fraction (data not shown). Although D447N ArsA is largely insoluble, the minor steady-state level of soluble D447N ArsA *in vivo* is probably enough to form a functional ArsAB pump, that provides resistance to arsenite, as shown in Figure 2B.

Wild type and altered ArsAs were purified by Ni^{2+} affinity chromatography to >95% homogeneity. Cells expressing

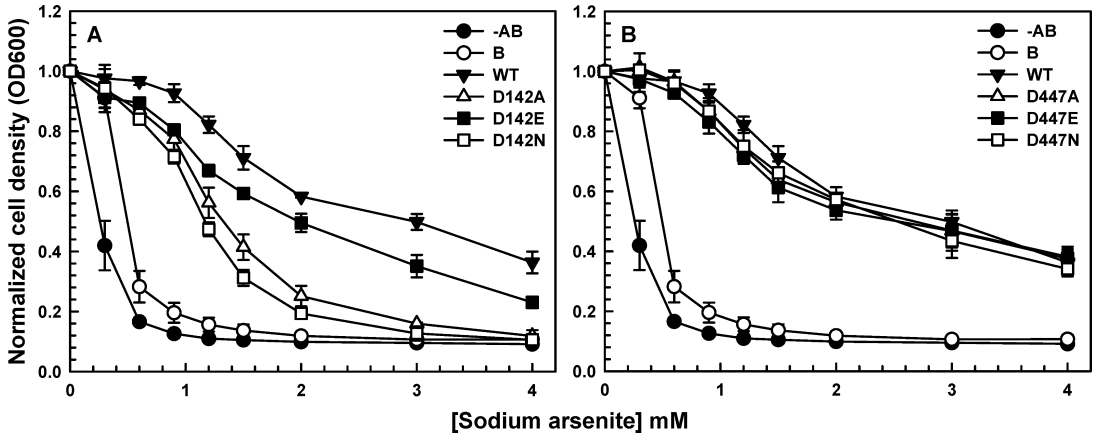

FIGURE 2: Resistance to arsenite in cells expressing wild type and altered ArsA proteins. Overnight cultures of *E. coli* strain JM109 bearing wild type and mutant *ars* plasmids were diluted 100-fold into fresh Luria−Bertani medium containing the indicated concentrations of sodium arsenite. Expression of the *ars* genes was induced with 0.1 mM IPTG. After 5 h of growth at 37 °C, the optical density at 600 nm was measured. Cells contained the following plasmids. Panel A: (▼) pTZ3H6 (*arsAB*), (Δ) pD142A ($arsA_{D142A}B$), (■) pD142E ($arsA_{D142E}B$), (□) pD142N ($arsA_{D142N}B$), (○) pALTER-B (*arsB*), and (●) vector plasmid pALTER-1. Panel B: (▼) pTZ3H6 (*arsAB*), (Δ) pD447A ($arsA_{D447A}B$), (■) pD447E ($arsA_{D447E}B$), (□) pD447N ($arsA_{D447N}B$), (○) pALTER-B (*arsB*), and (●) vector plasmid pALTER-1.

Table 2: V_{max} of Oxyanion-Stimulated ATPase Activity of ArsA Proteins

	V_{max} (nmol of ATP hydrolyzed/min/mg of protein)				
ArsA	−Sb(III) or −As(III)	+Sb(III)	fold stimulation by Sb(III)	+As(III)	fold stimulation by As(III)
wild type	100	1000	10	300	3
D142A	15	180	12	50	3.3
D142E	15	990	66	255	17
D142N	15	180	12	50	3.3
D447A	75	200	2.7	115	1.5
D447E	75	225	3	115	1.5

either the wild type or $arsA_{D142A}$, $arsA_{D142E}$, or $arsA_{D142N}$ genes consistently provided an average yield of 75 mg of pure protein per liter of culture. Under similar conditions only 15 mg of soluble protein was recovered from D447A or D447E expressing cells, so roughly only 20% of the D447A and D447E ArsA are present in the cytosolic fraction. The near complete insolubility of D447N ArsA precluded its purification and biochemical characterization.

Properties of Altered ArsAs. The altered ArsAs were analyzed for their ability to hydrolyze ATP in the presence of either antimonite or arsenite. In the absence of metalloids, the basal rate of ATPase activity of D142E ArsA was several-fold lower than the wild type (Table 2). In the presence of metalloids, and at high concentrations of Mg^{2+}, the maximal rate of ATP hydrolysis of the D142E enzyme was similar to that of the wild type. D142E ArsA showed a 4-fold increase in the K_m for ATP and activation required 4-fold higher Mg^{2+} concentration than the wild type (Table 3). This property is similar to that of mutants of Asp45, another ligand to the NBD1 Mg^{2+} (*12*). Additionally, the concentration of antimonite required for half-maximal activation increased by about 13-fold, while that for arsenite increased by approximately 4-fold.

The D142A and D142N enzymes showed approximately a 6-fold lowering in both the basal and metalloid-stimulated ATPase activity (Table 2). The affinity for ATP and antimonite was reduced by an order of magnitude (Table 3). Each of these altered proteins required approximately a 3-fold increase in arsenite concentration for half-maximal activation. When compared with wild type ArsA, the D142N enzyme exhibited a 25-fold increase in the concentration of Mg^{2+} required for half-maximal activation, while D142A ArsA exhibited a 60-fold increase. The kinetics of Mg^{2+} binding was also altered. Although both the wild type and D142E ArsA displayed apparent sigmoidal kinetics as a function of Mg^{2+} concentration, both D142A and D142N ArsA displayed classical hyperbolic kinetics (Figure 3). Also surprising was the fact that the hyperbolic substrate velocity curves for ATP, observed for both wild type and D142E ArsA, followed sigmoidal kinetics when Asp142 was altered to either alanine or asparagine (Figure 4).

D447A and D447E ArsA showed slightly lower basal ATPase activity than the wild type enzyme, but the activated rate was significantly lower (Table 2). Each of these altered proteins required several-fold increase in the concentration of ATP, Sb(III) or As(III) for activation (Table 3). Interestingly, the concentration of Mg^{2+} required for half-maximal activation was unaffected in D447A and D447E ArsA, and showed similar kinetics as the wild type enzyme (Figure 3). Also, D447A but not D447E ArsA exhibited apparent sigmoidal ATP kinetics as a function of ATP concentration (Figure 4).

Effect of Aspartate Substitutions on Accessibility to Trypsin. ArsA undergoes a number of conformational changes during the catalytic cycle (*15, 21–24*). We have used accessibility to trypsin as an indicator of conformation (*20, 25, 26*). Five general states of the enzyme can be distinguished by limited trypsin digestion. State one is an open conformation, in which the A1 and A2 halves are far enough apart to allow access to trypsin. This state is found under noncatalytic conditions in the absence of substrate or in the presence of metalloid or Mg^{2+} alone. In this open state, ArsA is extremely sensitive to trypsin digestion. Trypsin cleaves the ArsA at Arg290 to produce a 32 kDa A1 fragment that remains stable to trypsin digestion, and a slightly smaller A2 fragment which is digested rapidly (*27*). In the second state, observed in the presence of ATP alone (noncatalytic conditions), a 50 kDa fragment appears briefly, which is then rapidly digested to a ~30 kDa species. The third state is also observed under noncatalytic conditions but in the

Table 3: ArsA ATPase Kinetics

ArsA	ATP K_m (mM)	$[C]_{50\%activation}$ (mM)			Hill coefficient (Mg^{2+})
		Sb(III)	As(III)	Mg^{2+}	
wild type	0.035 ± 0.003	0.005 ± 0.001	0.7 ± 0.02	1.0 ± 0.1	2.8 ± 0.2
D142A	1.25 ± 0.3	0.1 ± 0.01	2.3 ± 0.4	62.5 ± 10	0.6 ± 0.05
D142E	0.15 ± 0.02	0.065 ± 0.004	2.6 ± 0.3	4.5 ± 0.2	2.2 ± 0.3
D142N	0.9 ± 0.03	0.1 ± 0.005	2.4 ± 0.4	27.0 ± 0.2	0.6 ± 0.1
D447A	0.6 ± 0.1	0.025 ± 0.002	3.4 ± 0.6	1.5 ± 0.2	2.2 ± 0.2
D447E	0.2 ± 0.04	0.025 ± 0.002	1.3 ± 0.2	1.0 ± 0.2	2.8 ± 0.2

presence of both ATP and metalloid. In this state, the rate of trypsin digestion is retarded, indicating that binding of both ATP and metalloid results in the formation of an interface between A1 and A2 that hinders access to trypsin. This effect of nucleotide and metalloid together is synergistic in that neither alone produces this conformation. The fourth state is a more closed conformation, observed in the presence of MgATP, that is, the enzyme is exhibiting basal ATPase activity. In this state, the rate of trypsin digestion is even more retarded than under noncatalytic conditions, suggestive of the formation of a different interface between A1 and A2. Finally, the fifth state is observed during metalloid stimulated catalysis. In this state, ArsA becomes resensitized to trypsin. The 63 kDa ArsA is cleaved to a 50 kDa species, which remains insensitive to trypsin digestion for a significant amount of time, indicating a different conformation of ArsA during metalloid stimulated activity. Our interpretation is that ArsA is alternating between open and closed conformations during activated catalysis. Thus, part of the time trypsin is excluded from the A1−A2 interface, and part of the time trypsin can proteolyze the surface of A2.

As discussed above, in the absence of substrates, wild type ArsA was rapidly cleaved by trypsin to one or more polypeptides of 30 kDa (*26*). Each altered protein exhibited a similar proteolytic pattern as the wild type (data not shown). Upon incubation of wild type ArsA with ATP followed by treatment with trypsin, a 50 kDa species was first observed that was subsequently cleaved to smaller fragments (Figure 5A). Each mutant protein exhibited similar protection from proteolytic digestion in the presence of ATP, indicating that the proteins adopt similar conformations as the wild type upon binding ATP (Figure 5B−F). Incubation with Sb(III) afforded no protection from proteolysis either with the wild type (*26*) or altered proteins (data not shown). The rate of cleavage was decreased synergistically when both ATP and Sb(III) were present together (Figure 5), suggesting that the enzyme adopts a trypsin-resistant conformation when both the MBD and NBDs are filled. The similarity in these trypsin proteolysis patterns indicates that the binding of ATP and Sb(III) elicits similar conformational changes in either wild type or altered ArsAs. Addition of Mg^{2+} alone had no effect on proteolysis (data not shown). ATP and Mg^{2+} together, which produces basal hydrolysis, also provided synergistic protection to wild type or mutant proteins (Figure 5). The full-length 63 kDa ArsA was cleaved to a 50 kDa species which remained intact for a significant amount of time in

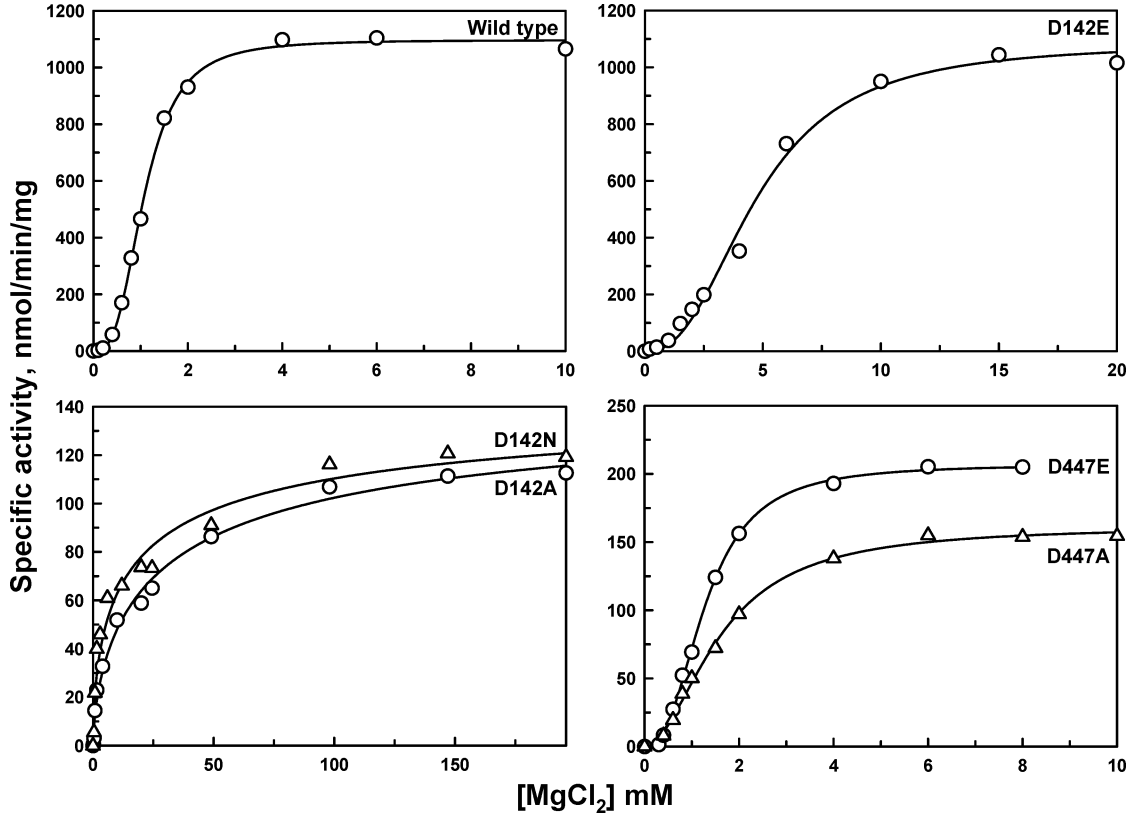

FIGURE 3: ArsA catalysis as a function of magnesium ion concentration in wild type and altered ArsAs. ATPase activity was measured at 37 °C, at the indicated concentrations of $MgCl_2$ (mM), using an NADH-coupled assay method (*19*). The basal ATPase activity was subtracted from each of the plots.

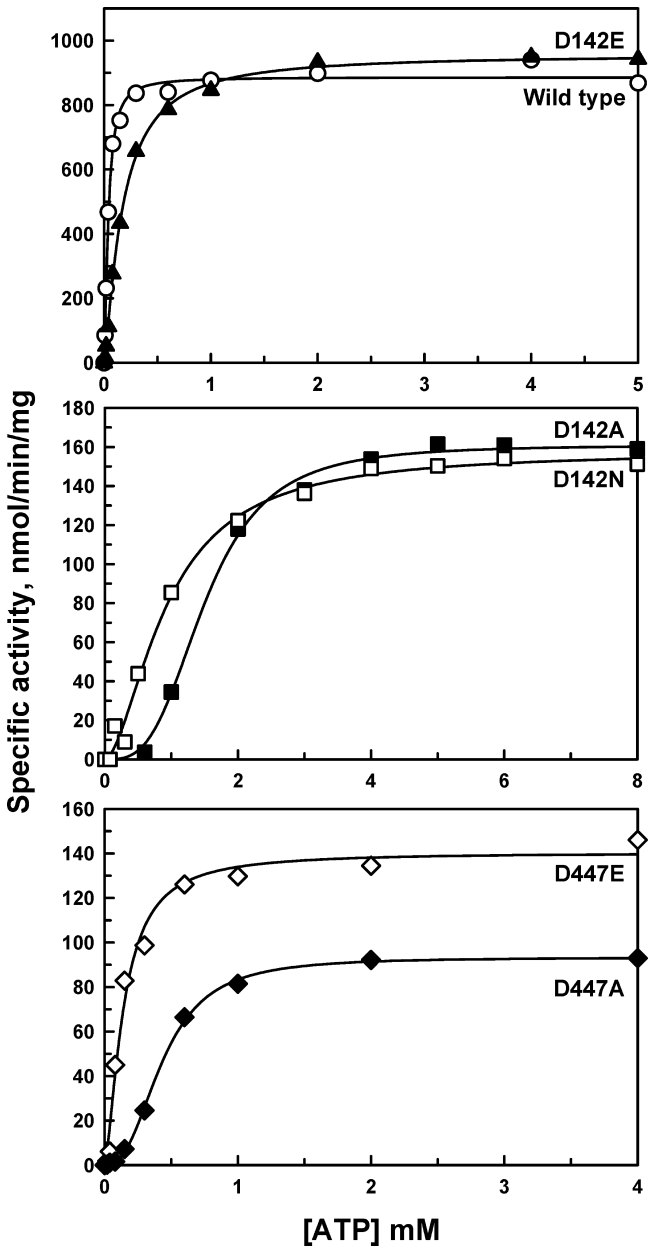

FIGURE 4: Kinetics of wild type and altered ArsAs as a function of ATP concentrations. ATPase activity was measured at the indicated concentrations of ATP (mM), at 37 °C, using an NADH-coupled assay method (*19*). The basal ATPase activity was subtracted from each of the plots.

the presence of both ligands (Figure 5). Thus the conformation of the wild type and mutant proteins, as detected by trypsin accessibility, seems to be similar during basal ATPase activity.

The trypsin digestion pattern was much different when all three ligands, ATP, Sb(III), and Mg^{2+}, were added together, conditions that produce activated catalysis. When the proteins were first incubated with ATP, Sb(III) and Mg^{2+}, and then treated with trypsin, wild type ArsA was rapidly digested to a 50 kDa species that was stable to further trypsin attack (Figure 5A). Both D142E and D447E showed a protracted proteolysis rate under similar conditions, with slow formation of the 50 kDa species (Figure 5C, 5F). In contrast, under similar conditions, D142A, D142N, and D447A ArsA exhibited greater stability of the full-length protein and no buildup of the 50 kDa species (Figure 5B, 5D, and 5E). Thus, the results of the trypsin sensitivity assays demonstrate that, although both Asp142 and Asp447 mutants behave similarly to the wild type during basal catalysis, the D142A, D142N, and D447A ArsA acquire a different conformation during metalloid-stimulated catalysis.

Effect of Aspartate Substitution on Intrinsic Trp159 Fluorescence. The crystal structure of ArsA with ADP bound at the two NBDs (*8*) indicates Trp159 to be 29.1 Å and 37.8 Å from Asp142 and Asp447, respectively. Analysis of the different crystal forms of ArsA with ADP bound at NBD1 and ATP, AMP-PNP, or ADP·AlF_3 bound at NBD2 (*10*), depicts negligible shifts in the position of Trp159 with respect to either Asp142 or Asp447. Under these crystallographic conditions, Trp159 seems to be positioned in a relatively hydrophilic environment, the closest residues being Gln154, Leu155, Lys181, Gln182, Arg183, and several water molecules. Fluorescence experiments also indicate Trp159 to reside in a relatively hydrophilic environment (*15*). An increase in intrinsic tryptophan fluorescence and a blue shift of the maximum emission wavelength were observed upon addition of MgATP, indicating movement of Trp159 into a relatively less polar environment. No fluorescence response was observed with MgADP or nonhydrolyzable ATP analogues, suggesting that Trp159 shifts only during ATP hydrolysis (*15*). Upon addition of Sb(III) to the MgATP form, which activates hydrolysis, the fluorescence is rapidly and dramatically quenched, so Trp159 must become solvent exposed. Note that this is the form in which ArsA was crystallized, and Trp159 is surface localized in this structure.

When excited at 295 nm, Trp159 of the wild type ArsA has an emission maximum at 337 nm in its native state, while the denatured protein has an emission maximum at 353 nm (*15*). Each of the Asp142 and Asp447 mutants has the same emission maximum as the parental ArsA (Figure 6A), again indicating that substitution at Asp142 or Asp447 with Ala, Asn or Glu has little effect on the environment of Trp159. Addition of MgATP to wild type ArsA resulted in a marked increase in fluorescence (Figure 6B). This metalloid-independent fluorescence enhancement occurs only during basal catalysis and has been interpreted as a slow conformational change in the enzyme to a highly fluorescent intermediate that is rate-limiting for ATP hydrolysis (*24, 28*). The enhancement is reversed by addition of Sb(III) (Figure 6B). The reversal by metalloid results from increasing the rate of isomerization between the highly fluorescent intermediate and the initial state of ArsA such that this step is no longer rate-limiting for hydrolysis, allowing for activated catalysis (*23*). Since Asp447 mutants show similar basal ATPase activity as the wild type (Table 2), we expected a marked increase in fluorescence upon addition of MgATP to either D447A or D447E ArsA. Interestingly, none of the Asp142 and Asp447 mutants responded to the addition of MgATP or Sb(III), in spite of the fact that each exhibits basal and activated ATPase activity (Table 2). Our interpretation of the results is that Trp159 no longer reports hydrolysis upon alteration of either Asp142 or Asp447.

DISCUSSION

The crystal structure of ArsA ATPase revealed that Asp142 of STD1 and Asp447 of STD2 are coordinated indirectly to Mg^{2+} through water molecules (*8*) (Figure 1).

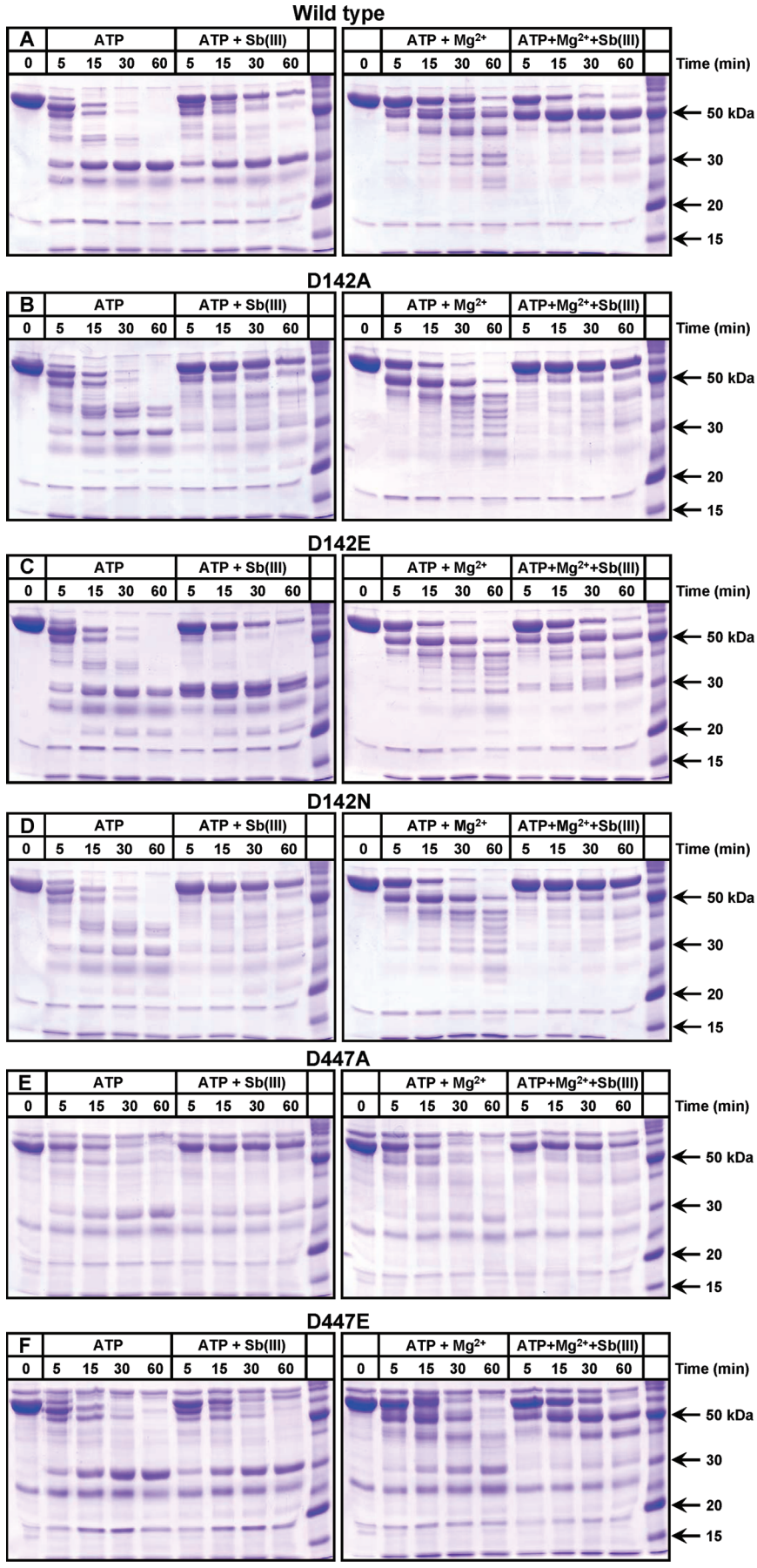

FIGURE 5: Effect of alteration of Asp142 or Asp447 on accessibility to trypsin. Trypsin digestion was performed at room temperature with the indicated additions: 5 mM ATP, 0.5 mM potassium antimonyl tartrate (Sb(III)), or 5 mM $MgCl_2$. ArsA proteins were treated with trypsin as described in Experimental Procedures. At the indicated times, samples were removed, and the reactions were terminated by the addition of soybean trypsin inhibitor. The tryptic products were analyzed by 12% SDS−PAGE and stained with Coomassie Blue. The positions of migration of standards are indicated.

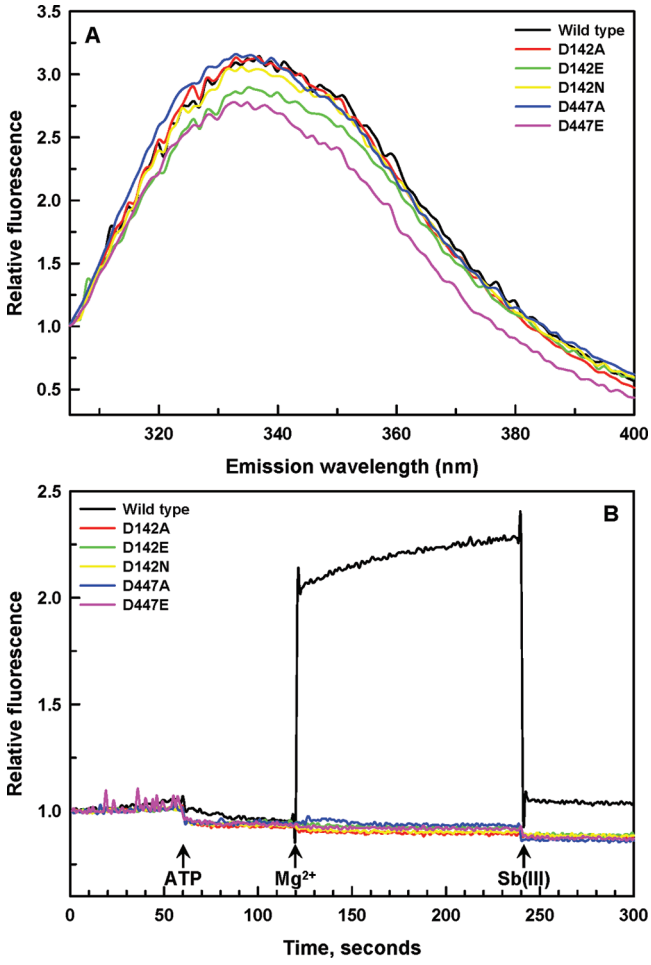

FIGURE 6: Effect of alteration of Asp142 or Asp447 on intrinsic Trp159 fluorescence. A. Emission spectra of Trp159 in wild type and altered ArsAs. B. Response of Trp159 fluorescence upon addition of ATP, Mg^{2+}, and Sb(III) in wild type and altered ArsAs. At the indicated times, 5 mM ATP, 5 mM Mg^{2+}, and 1 mM Sb(III) were added to 1.3 μM ArsA.

In that report, both Asp142 and Asp447 were hypothesized to be the primary effectors of information flow between the two NBDs and the MBD. We propose that the conserved aspartates might have two functions. First, since Asp142 and Asp447 each serve as a ligand to MgATP, they may play a role in Mg^{2+} binding. Second, as Asp142 and Asp447 form the N-terminal end of the $D_{142/447}$TAPTGH$_{148/453}$ sequence, they may play a role in signal transduction between the NBDs and MBD. The goal of this study was to examine what role the two aspartates play in Mg^{2+} binding, signal transduction, and hence, catalysis.

Several lines of evidence indicate that substitution of Asp142 or Asp447 with Ala, Asn or Glu residues did not affect the overall conformation. First, the altered proteins were produced in normal amounts and were not degraded *in vivo* (data not shown). Second, the fluorescence emission spectra of each of the mutants were superimposable, indicating that the environment of Trp159 was the same for each protein (Figure 6A). And finally, trypsin digestion experiments in the presence of ATP and Sb(III) clearly showed that there were minimal differences between wild type and altered ArsAs under noncatalytic conditions (states 1, 2, and 3). The overall similarity in the proteolysis pattern indicates that the mutants retain ability to bind ATP and Sb(III) (Figure 5).

At early times, MgATP (basal activity) also provided similar levels of protection to both wild type and altered ArsAs (state 4). However, upon prolonged incubation, the altered ArsAs appear to be more sensitive to trypsin cleavage than wild type (Figure 5). This would indicate that the altered proteins adopt a more open conformation during basal catalysis, rendering them more accessible to protease than the wild type protein. Only under activated conditions (state 5) did the altered ArsAs exhibit significant differences in sensitivity to trypsin proteolysis when compared to the wild type (Figure 5). Wild type ArsA became more sensitive to trypsin under metalloid stimulated conditions [MgATP and Sb(III)] than under basal conditions (MgATP), consistent with our suggestion that the interface between A1 and A2 is alternatively accessible and inaccessible to trypsin during the activated catalytic cycle. Both D142E and D447E ArsA showed a retarded rate of proteolysis, with slower generation of the 50 kDa fragment, which was subsequently cleaved to lower molecular weight species. In contrast, D142A, D142N, and D447A ArsA adopted a remarkably trypsin-resistant conformation under activated conditions, indicating that the interface between A1 and A2 in these mutants remained closed and inaccessible to trypsin.

Evidence for local conformational changes also came from kinetic studies. Although the significance of the apparent cooperativity is not clear, mutation of Asp142 to either alanine or asparagine converted the Mg^{2+}-dependent substrate-velocity kinetics from sigmoidal to hyperbolic curves. Also, the ATP-dependent kinetics switched from hyperbolic to sigmoidal for both D142A and D142N ArsA. It is likely that mutation of Asp142 produces a local conformational change in A1, which is transmitted to A2, affecting the interaction between the two halves of ArsA, as reflected by their increased protection from trypsin digestion under catalytic conditions. Alteration of Asp447 to alanine or glutamate showed a trypsin digestion pattern similar to that of the Asp142 counterpart. Mutation of Asp447 converted the kinetics from hyperbolic to sigmoidal, a phenomenon similar to that observed for D142A and D142N ArsA. Interestingly, the Asp447 mutants exhibited Mg^{2+}-dependent substrate kinetics similar to that of the wild type. Taken together the evidence indicates that the Asp447 mutants adopt a slightly different conformation than the Asp142 mutants.

Further evidence of local conformational changes came from fluorescence experiments. In the absence of ligands, each of the Asp142 and Asp447 mutants exhibited Trp159 fluorescence similar to that of the wild type (Figure 6A). However, the enhancement of fluorescence upon addition of ATP and Mg^{2+} was lost for both Asp142 and Asp447 mutants (Figure 6B). Why does Trp159 fluorescence not report signal transduction in these mutants? Very likely, alteration of either of the aspartates produces a local conformational change that does not allow the buildup of the highly fluorescent conformation, which is rate-limiting for the wild type (*22*). Thus alteration of either Asp142 or Asp447 affects communication between the metal and catalytic center.

The crystal structure of ArsA shows that both Asp142 and Asp447 are liganded to Mg^{2+} through water molecules. It is possible that alteration of either residue would affect their affinity for Mg^{2+}. Alteration of Asp142 to Glu, Asn or Ala decreased the affinity for Mg^{2+} by approximately 4-, 25-,

and 60-fold, respectively. This is also reflected in the phenotypic assays. The concentration of soluble Mg^{2+} in *E. coli* is approximately 4 mM (*29*), which is sufficient to support D142E ATPase activity (Table 3), but not D142A and D142N ArsA, which require much higher concentrations of Mg^{2+} for half-maximal activation (Table 3). Consequently, cells expressing D142E ArsA show slightly lower sensitivity than wild type, whereas both D142A and D142N expressing cells were considerably less resistant to arsenite than wild type (Figure 2). By the same token, both D447A and D447E ArsA showed similar affinity for Mg^{2+} as the wild type, and cells expressing these proteins exhibited similar arsenite resistance. Therefore, Asp142 but not Asp447 appears to be involved in Mg^{2+} binding.

Both Asp142 and Asp447 mutants showed basal and activated ATPase activity (Table 2). Although the activities of most of the mutants were several-fold lower than the wild type, the mutant enzymes are still functional ATPases, indicating that neither Asp142 nor Asp447 is required for catalysis. This should not be surprising since both Asp142 and Asp447 are only one of six Mg^{2+} ligands (*8*) (Figure 1). Since only D142E exhibited metalloid-stimulated ATP hydrolysis at rates equivalent to wild type ArsA, an acidic residue at position 142 may be necessary for metalloid-stimulated activity.

More interestingly, alteration of Asp142 significantly decreased the affinity for both ATP and metalloid (Table 3). We interpret the lower affinity for nucleotide as a direct result of the lower affinity for Mg^{2+}. Since Asp142 is the N-terminal end of the signal transduction sequence that reciprocally transmits information between the NBDs and MBD, lower affinity for MgATP results in simultaneous lower affinity for Sb(III), indicating again that Asp142 plays a role in signal transduction. On the other hand, although the affinity for Mg^{2+} remains the same as wild type for each of the Asp447 mutants, they still show a reduction in affinities for ATP and Sb(III). One possibility is that local conformational changes associated with changing Asp447 impede signal transduction between MBD and NBD2, thereby affecting binding of nucleotide and metalloid. The occurrence of local conformational changes accompanying the mutations is supported by the trypsinization experiments, where a decrease in activation is inversely related to a trypsin-resistant conformation. On the other hand, each Mg^{2+} is coordinated by multiple water and protein ligands, so the effect of loss of a single indirectly coordinated ligand such as Asp447 may not be easily quantified but still affect the affinity for other ligands. Why do the Asp447 mutants exhibit similar phenotype as the wild type although they show decreased affinities for both nucleotide and metalloid? The relationship between phenotype and biochemical activity is difficult to quantify. For example, the activity of purified ArsA is assayed in the absence of ArsB, whereas the phenotype data represents an *in vivo* ArsA−ArsB interaction. Since ArsB is difficult to purify, it has not been possible to determine how interaction with ArsB affects the kinetic parameters of ArsA mutants.

In conclusion, the results demonstrate that Asp142 and Asp447 have different roles in ArsA catalysis. Since substitution of Asp142 with nonacidic residues clearly affects Mg^{2+} binding, a major function is most likely in stabilization of bound MgATP in NBD1. Asp142 also plays a role in transduction of the signal of Sb(III) binding, i.e., the ability of hydrolysis to be stimulated by metalloid. In contrast, the role of Asp447 in Mg^{2+} binding is not as critical as that of Asp142, as alterations in Asp447 do not affect the kinetics of enzyme activity as a function of Mg^{2+} concentration. However, Asp447 is most likely involved in reciprocal transmission of information on the ligand occupancy of NBD2 and the MBD. We have earlier shown that substitution of His148 at the C-terminal end of STD1 affects communication between NBD1 and MBD, and likewise alteration of His447 at the C-terminal end of STD2 affects communication between MBD and NBD2 (*13*). The roles of other residues in the two STDs in ArsA catalysis are currently being investigated.

ACKNOWLEDGMENT

We thank Dr. S. Thiyagarajan for structural analysis.

REFERENCES

1. Abernathy, C. O., Thomas, D. J., and Calderon, R. L. (2003) Health effects and risk assessment of arsenic. *J. Nutr. 133*, 1536S–1538S.
2. Bhattacharjee, H., and Rosen, B. P. (2007) Arsenic Metabolism in Prokaryotic and Eukaryotic Microbes, in *Molecular Microbiology of Heavy Metals* (Nies, D. H. , and Silver, S., Eds.) pp 371−406, Springer, Berlin/Heidelberg.
3. Tisa, L. S., and Rosen, B. P. (1990) Molecular characterization of an anion pump. The ArsB protein is the membrane anchor for the ArsA protein. *J. Biol. Chem. 265*, 190–194.
4. Rosen, B. P., Weigel, U., Karkaria, C., and Gangola, P. (1988) Molecular characterization of an anion pump. The *arsA* gene product is an arsenite (antimonate)-stimulated ATPase. *J. Biol. Chem. 263*, 3067–3070.
5. Li, J., and Rosen, B. P. (2000) The linker peptide of the ArsA ATPase. *Mol. Microbiol. 35*, 361–367.
6. Karkaria, C. E., Chen, C. M., and Rosen, B. P. (1990) Mutagenesis of a nucleotide-binding site of an anion-translocating ATPase. *J. Biol. Chem. 265*, 7832–7836.
7. Kaur, P., and Rosen, B. P. (1992) Mutagenesis of the C-terminal nucleotide-binding site of an anion-translocating ATPase. *J. Biol. Chem. 267*, 19272–19277.
8. Zhou, T., Radaev, S., Rosen, B. P., and Gatti, D. L. (2000) Structure of the ArsA ATPase: the catalytic subunit of a heavy metal resistance pump. *EMBO J. 19*, 4838–4845.
9. Ruan, X., Bhattacharjee, H., and Rosen, B. P. (2008) Characterization of the metalloactivation domain of an arsenite/antimonite resistance pump. *Mol. Microbiol. 67*, 392–402.
10. Zhou, T., Radaev, S., Rosen, B. P., and Gatti, D. L. (2001) Conformational changes in four regions of the *Escherichia coli* ArsA ATPase link ATP hydrolysis to ion translocation. *J. Biol. Chem. 276*, 30414–30422.
11. Jiang, Y., Bhattacharjee, H., Zhou, T., Rosen, B. P., Ambudkar, S. V., and Sauna, Z. E. (2005) Nonequivalence of the nucleotide binding domains of the ArsA ATPase. *J. Biol. Chem. 280*, 9921–9926.
12. Zhou, T., and Rosen, B. P. (1999) Asp45 is a Mg^{2+} ligand in the ArsA ATPase. *J. Biol. Chem. 274*, 13854–13858.
13. Bhattacharjee, H., and Rosen, B. P. (2000) Role of conserved histidine residues in metalloactivation of the ArsA ATPase. *Biometals 13*, 281–288.
14. Sambrook, J., and Russell, D. (2001) *Molecular Cloning: A Laboratory Manual*, 3rd ed., Cold Spring Harbor Laboratory Press, Cold Spring Harbor, NY.
15. Zhou, T., and Rosen, B. P. (1997) Tryptophan fluorescence reports nucleotide-induced conformational changes in a domain of the ArsA ATPase. *J. Biol. Chem. 272*, 19731–19737.
16. Chung, C. T., Niemela, S. L., and Miller, R. H. (1989) One-step preparation of competent *Escherichia coli*: transformation and storage of bacterial cells in the same solution. *Proc. Natl. Acad. Sci. U.S.A. 86*, 2172–2175.
17. Laemmli, U. K. (1970) Cleavage of structural proteins during the assembly of the head of bacteriophage T4. *Nature 227*, 680–685.

18. Bhattacharjee, H., and Rosen, B. P. (2001) Structure-function analysis of the ArsA ATPase: contribution of histidine residues. *J. Bioenerg. Biomembr. 33*, 459–468.
19. Kuroda, M., Bhattacharjee, H., and Rosen, B. P. (1998) Arsenical pumps in prokaryotes and eukaryotes. *Methods Enzymol. 292*, 82–97.
20. Hsu, C. M., and Rosen, B. P. (1989) Characterization of the catalytic subunit of an anion pump. *J. Biol. Chem. 264*, 17349–17354.
21. Zhou, T., Liu, S., and Rosen, B. P. (1995) Interaction of substrate and effector binding sites in the ArsA ATPase. *Biochemistry 34*, 13622–13626.
22. Walmsley, A. R., Zhou, T., Borges-Walmsley, M. I., and Rosen, B. P. (1999) The ATPase mechanism of ArsA, the catalytic subunit of the arsenite pump. *J. Biol. Chem. 274*, 16153–16161.
23. Walmsley, A. R., Zhou, T., Borges-Walmsley, M. I., and Rosen, B. P. (2001) Antimonite regulation of the ATPase activity of ArsA, the catalytic subunit of the arsenical pump. *Biochem. J. 360*, 589–597.
24. Walmsley, A. R., Zhou, T., Borges-Walmsley, M. I., and Rosen, B. P. (2001) A kinetic model for the action of a resistance efflux pump. *J. Biol. Chem. 276*, 6378–6391.
25. Kaur, P. (1999) The anion-stimulated ATPase ArsA shows unisite and multisite catalytic activity. *J. Biol. Chem. 274*, 25849–25854.
26. Ruan, X., Bhattacharjee, H., and Rosen, B. P. (2006) Cys-113 and Cys-422 form a high affinity metalloid binding site in the ArsA ATPase. *J. Biol. Chem. 281*, 9925–9934.
27. Ramaswamy, S., and Kaur, P. (1998) Nucleotide binding to the C-terminal nucleotide binding domain of ArsA: Studies with an ATP analogue, 5′-*p*-fluorosulfonylbenzoyladenosine. *J. Biol. Chem. 273*, 9243–9248.
28. Rosen, B. P., Bhattacharjee, H., Zhou, T., and Walmsley, A. R. (1999) Mechanism of the ArsA ATPase. *Biochim. Biophys. Acta 1461*, 207–215.
29. Lusk, J. E., Williams, R. J., and Kennedy, E. P. (1968) Magnesium and the growth of Escherichia coli. *J. Biol. Chem. 243*, 2618–2624.
30. Li, J., Liu, S., and Rosen, B. P. (1996) Interaction of ATP binding sites in the ArsA ATPase, the catalytic subunit of the Ars pump. *J. Biol. Chem. 271*, 25247–25252.

BI800715H